Land cover classification of a non-accessible area using multi-sensor images and GIS data

다중센서와 GIS 자료를 이용한 접근불능지역의 토지피복 분류

Yongmin Kim[1] · Wanyong Park[2] · Yangdam Eo[3] · Yongil Kim[4]

김용민 · 박완용 · 어양담 · 김용일

Abstract

This study proposes a classification method based on an automated training extraction procedure that may be used with very high resolution (VHR) images of non-accessible areas. The proposed method overcomes the problem of scale difference between VHR images and geographic information system (GIS) data through filtering and use of a Landsat image. In order to automate maximum likelihood classification (MLC), GIS data were used as an input to the MLC of a Landsat image, and a binary edge and a normalized difference vegetation index (NDVI) were used to increase the purity of the training samples. We identified the thresholds of an NDVI and binary edge appropriate to obtain pure samples of each class. The proposed method was then applied to QuickBird and SPOT-5 images. In order to validate the method, visual interpretation and quantitative assessment of the results were compared with products of a manual method. The results showed that the proposed method could classify VHR images and efficiently update GIS data.

Keywords : Classification, Automated training, multi-sensor images, non-accessible area

1. Introduction

Land cover is useful information to carry out military operations and it requires regular updating of a land cover database for accurate and timely geospatial information (Park et al. 2009). To quantify database change, many components have to be considered because they are abstract and subjective (Kim 2008). While geospatial information of most areas is easily obtained, it is difficult to get and update in non-accessible areas such as a demilitarized zone (DMZ), because of military agreements prescribing access-denied and aircraft-denied areas in DMZs. In this case, maps relying on satellite remote-sensing data have many advantages because they can obtain data for any large areas without the limitations of approaches relying on closer proximity. In particular, commercially avail-

able very high resolution (VHR) images, obtained from QuickBird, IKONOS, KOMPSAT-2, and SPOT-5, etc., can provide a large amount of ground surface information in a timely manner (Huang et al. 2007). Therefore, these images allow the generation of geometrically detailed land cover maps. Many studies have proven the use of VHR imagery in updating large-scale thematic maps through diverse supervised classification approaches (Davis et al. 2002; Tarantino et al. 2003). Supervised classification or manual classification performed by a trained expert is labour intensive, highly subjective, and non-reproducible (Zijdenbos et al. 1998; Zijdenbos et al. 2002) because such classification involves time consuming and detailed image extraction work performed by an operator with a lot of experience (Walter 1998). In addition, even though each analyst extracts training data

from each of the classes, there are always differences among them because the analysts do not have the same level of expertise (Eo 1999). Thus, all of the aforementioned factors play a role in decreasing the accuracy and reliability of the classification results.

Classification that does not need the intervention of an operator can be an effective alternative because it can retain the constancy of classification results. In addition, it can be effective in saving time by automatically extracting training data without operator intervention. Therefore, many automatic classification methods have been proposed. In particular, the approach utilizing geographic information system (GIS) data, like a land cover map, has been studied because of the advantage that an operator can easily handle and refer to attributes of the GIS data. GIS data are generally used as a knowledge to identify some of the features and as an input data to automatically extract training data in a supervised classification process (Walter 1998; Di et al. 2000; Yang 2007; Eo et al. 2008; Maselli et al. 2008). These methods using GIS data can replace the manual sampling process required by the supervised classification procedure for obtaining the parameters. In addition, many studies have proposed the use of GIS data as a logical channel or a prior probability (Maselli et al. 1992; Ricchetti 2000; Chen and Stow 2003; Kim et al. 2009a). These methods improve the classification accuracy by providing some information to the analyst and the classifier used.

However, these methods are difficult to use when there is a scale difference between the VHR image and the GIS data to be used for generating pure training samples of each class in a VHR image. Also, many applications of traditional single-resolution classification approaches have led to unsatisfactory results due to the more heterogeneous spectral-radiometric characteristics within land-use or land-cover features portrayed in VHR images (Barnsley and Barr 1996). Thus, the objective of this paper is to propose a classification method based on an automated training extraction procedure to overcome scale differences between VHR images and GIS data.

The remainder of the paper is organized as follows. In Section 2, the experimental site and source data selected for this paper are explained. In Section 3, the automated training extraction method that can adapt to a VHR image using GIS data is discussed. In Section 4, two application examples are described and the results are presented. Discussion with concluding remarks is presented in Section 5.

2. Experimental site and data source

2.1 Experimental site

The DMZ between South Korea and North Korea forbids entry by a private citizen and restrains most developments as a military buffer zone. This DMZ is an almost perfect natural environment, which is very rare, and many researchers are studying this area.

In this paper, we selected two experimental sites located in DMZs of Korea. The first site was Yeoncheon (100 km²) in South Korea, which includes an agricultural area, water, a built-up area, grass, and a forest feature. The second site was Cheorwon (64 km²) in South Korea, which includes four land cover classes but no grass features (Fig. 1). There are also the Tae-Pung observatory and a ceasefire line in these sites.

2.2 Data source

The proposed method used three data sources: a military digital map (MDM), Landsat image, and VHR image. These data are of different spatial resolution to each other. Table 1 presents information of datasets used in this paper. Although there is a difference of acquisition time among data, we assume that there is little land cover change because of the restraint of development in the DMZ.

The MDM consists of small-scale vector data and provides land cover and land use information for military operations in non-accessible areas. The feature codes of the MDM follow feature attribute coding catalogue guidelines, and are categorized as built-up, water, crop, grass, and forest (table 2). The MDM used in this paper was acquired in 2003 and covers two experimental sites. Due to military agreements concerning the access-denied and aircraft-denied areas in DMZs, it is difficult to update and revise. In the case of site 2, there were even areas that did not have attributes in the MDM.

Landsat Thematic Mapper (TM), a middle resolution imager (spatial resolution equal to 30 m), is a multispectral scanning radiometer that was carried on board Landsat 4 and

5. TM data cover the visible, near-infrared, shortwave, and thermal infrared spectral bands of the electromagnetic spectrum.
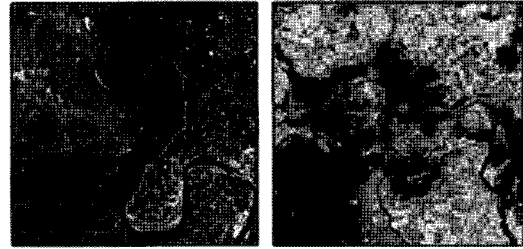
Launched on October 18, 2001, QuickBird collects multispectral and panchromatic imagery concurrently, and pan-sharpened products in natural or infrared colours are available. The multispectral products cover the visible and near-infrared wavelengths in four bands. Basic Imagery products are delivered at the resolution at which the data were collected (ranging from 2.44 to 2.88 m), while Standard and Ortho Imagery products are resampled to a 2.4 or 2.8 m pixel spacing. SPOT-5 was launched on May 4, 2002, and offers a resolution of 2.5-5 m in panchromatic mode and 10 m in multispectral mode. Ten-metre colour products are derived from multispectral images acquired simultaneously in the same four spectral bands. Bands B1, B2, and B3 yield images at a resolution of 10 m; the SWIR band yields 20 m images, which are then resampled to obtain a 10 m image.

Table 1. Information of dataset

Sensor /Source	Spatial Resolution	Time	Location
QuickBird	2.8 m	August 2004	Yeoncheon in South Korea
SPOT-5	10 m	October 2005	Cheorwon in South Korea
Landsat TM	30 m	June 2004	Above two sites
MDM	1:50 000 (scale)	2003	Above two sites

(a) QuickBird image of site 1   (b) SPOT-5 image of Cheorwon.

Fig. 1. Experimental sites

3. Proposed methods

3.1 Overview

This paper proposed a classification method based on an automated training extraction procedure to overcome a scale difference between VHR images and GIS data. The proposed method consists of three processes, a flowchart of which is given in Fig. 2. The first step is to conduct a maximum likelihood classification (MLC) of a Landsat image by using an MDM as input data. The second step is to extract training samples through filtering methods with binary edge and normalized difference vegetation index (NDVI) maps. Finally, the classification of a VHR image is conducted using the training parameters extracted in the following step. All of the processes were automated and conducted using the MATLAB R2008a program and ENVI 4.5 software with a Windows XP operating system.

Table 2. MDM feature code and definition

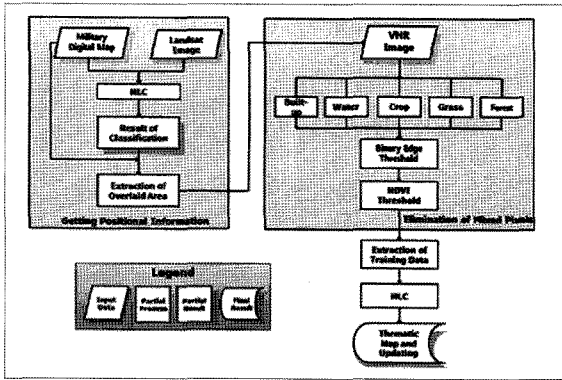| Integrated Class	Feature Code	Definition
Built-up	AL020	An area containing a concentration of buildings and other structures
Water	SA010	An area containing any surface water that is flowing or free standing such as lakes, rivers, oceans, reservoirs, etc
	BH140	A natural flowing watercourse
	BH090	An area periodically covered by flood water, excluding tidal waters
Crop	EA010	An area that has been tilled for the planting of crops
	BH135	An area periodically covered with water used for growing rice
Grass	EB020	Low-growing woody plants
	EB010	An area composed of uncultured plants that have little or no woody tissue
Forest	EC030	Woody perennial plants, having a self-supporting main stem or trunk

Fig. 2. Flowchart of the classification method based on the automated training extraction procedure.

3.2 Classification of the Landsat image using the MDM

It is difficult to directly enter attributes of the MDM as input data to automate the procedure of extracting training samples of a VHR image due to the scale differences between the MDM and the VHR image. Therefore, the use of a Landsat image may overcome this problem. The results of the MLC of the Landsat image play a role in the proposed method.

In order to conduct an MLC of the Landsat image, the attributes of the MDM were used as training data and prior probabilities. The prior probabilities of each class were calculated by the area proportion of the feature codes on the MDM. Six bands of the Landsat data were applied to conduct MLC omitting the thermal band.

3.3 Problem of spatial resolution difference between data

For classification of the VHR image, the training samples were collected by extracting pixels from the VHR image corresponding to pixels of the Landsat image that were correctly classified according to comparison with attributes of the MDM. It is very important that the quality of training samples is high to support the MLC of the VHR image. However, there are limits in terms of acquiring the pure training data of each class because of the spatial resolution differences between the Landsat and VHR images (Fig. 3). In one pixel of a Landsat image, there are many VHR pixels having different land cover features. Thus, the VHR image pixels of other classes located in one pixel of the Landsat image should be

removed in order to obtain pure training data for a specific class. The proposed method removes these pixels to minimize their influence by using binary edge and NDVI maps. In Sections 3.4 and 3.5, generation of the binary edge and NDVI maps is explained.
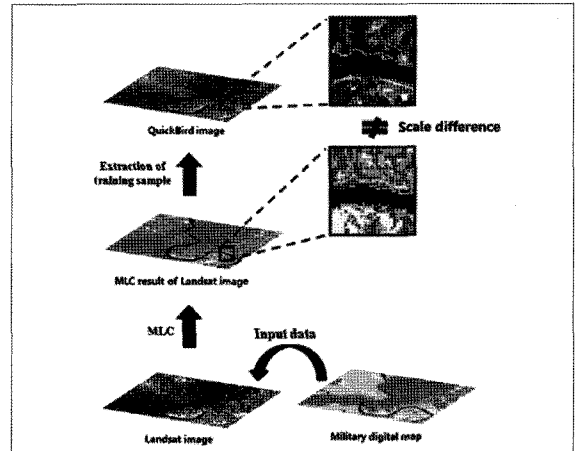

Fig. 3. Problem generated by scale difference between Landsat image and VHR image.

3.4 Generation of the binary edge map

The binary edge map was generated by extracting an edge from the second band, which showed the greatest contrast in the QuickBird and SPOT-5 images. The procedure for generating the binary edge map involved four steps:

(1) Application of Laplacian high-pass filter;

(2) Transformation to grey scale;

(3) Thresholding;

(4) Application of morphological filter.

At step 1, a Laplacian high-pass filter was applied to the VHR image (Fig. 4(b)). This filter enhances the high frequency components of an image in all directions. In this study, we used 7 by 7 window sizes. The components of the filter are shown in Fig. 4(d). At step 2, the results of step 1 were transformed to grey scale (0-255) to apply a threshold. At step 3, if the value of an edge was either below 24 or above 231, the value was changed to 255 and the other values were changed to 0 in order to construct a binary map. Finally, a binary edge map was generated by applying a 'closing' process, a morphological filter (Fig. 4(c)). The binary edge map can be used

to identify a built-up area, such as road, of the VHR image in the automated training procedure.
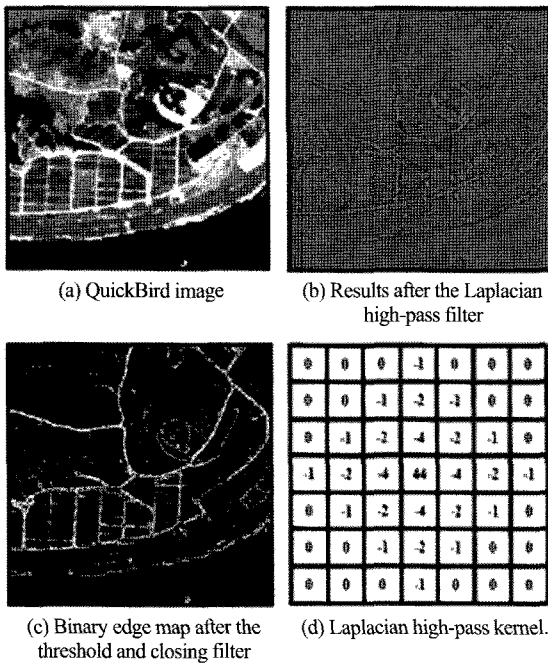

(a) QuickBird image

(b) Results after the Laplacian high-pass filter

(c) Binary edge map after the threshold and closing filter

(d) Laplacian high-pass kernel.

Fig. 4. Generation of the binary edge map.

3.5 Setting of forest threshold (FT) in the NDVI map

The NDVI is the most well known and widely used ratio-based index and is frequently used as a device to detect the activation rate of vegetation (Rouse et al. 1974). In addition, it is used as a threshold baseline to classify land cover (Wang and Tenhunen 2004; Haiping et al. 2006). In this paper, the NDVI plays an important filter role to distinguish some classes in conjunction with the binary edge map.

In general, in an NDVI map, non-vegetated surfaces are negative values, while vegetated ones are positive. In areas where vegetation canopies do not achieve absolute coverage, the NDVI is susceptible to the spectral influence of the soil, giving the possibility of uncertainties in interpretation (Peters and Eve 1995). However, this effect can also increase the NDVI of certain vegetated surfaces, and could potentially improve the separation of land cover classes. In particular, it is usefully utilized in the case of evergreens. Evergreens are characterized by very high positive NDVI values and they are located in a higher his-

togram position than other vegetation features regardless of the season (Martinuzzi et al. 2008). This is important in choosing the threshold of the NDVI in that there are many evergreens in DMZs of Korea during the four seasons.

After investigating a number of satellite images of non-accessible areas, the forest threshold (FT) was set as including the top 0.08% of the NDVI values. Using this criterion, 0.8 of site 1 and 0.13 of site 2 were assessed as evergreen forest (Fig. 5 and Fig. 6). We visually confirmed that pixels that had an NDVI value higher than the FT are the forest feature (red and blue points in Fig. 5(d) and 6(d)). There was a difference between the values of the FT for site 1 and site 2 because there was a seasonal change of two months.

Fig. 5. Setting of FT for site 1.
(a) NDVI map, (b) Histogram of NDVI map, (c) Magnified image of red box (3, 2, 1 band composite), (d) Pixels having NDVI value higher than FT (red points).
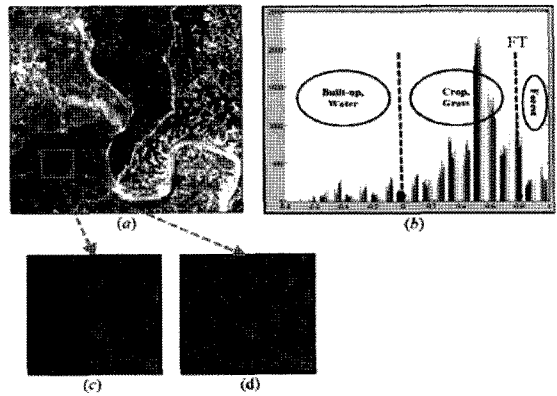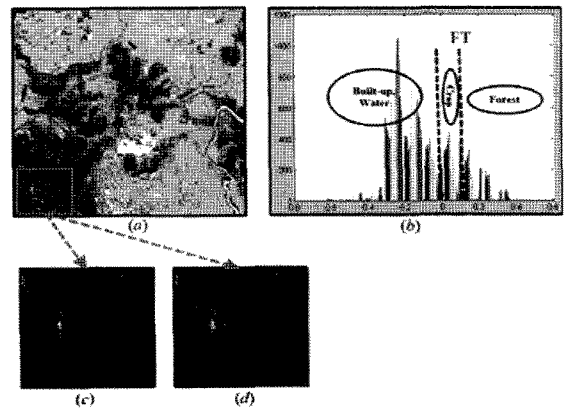

Fig. 6. Setting of FT for site 2.
(a) NDVI map, (b) Histogram of NDVI map, (c) Magnified image of red box (3, 2, 1 band composite), (d) Pixels having NDVI value higher than FT (blue points).

3.6 Automatic extraction of training samples

Filtering is good for extracting specific features and objects that an analyst wants and it is used in various fields such as road extraction, fire, and red tide detection in addition to classification (Zhu *et al.* 2005; Han and Lee 2006; Kim *et al.* 2009b). This paper uses a filtering method to automatically extract training samples for classification. The process is an important part of the proposed method for conducting an MLC of the VHR images because the higher the quality of the training samples, the better the results of the classification. The process of "automated extraction method of training sample for VHR image" occurs in the following steps:

(1) Extraction of latent training samples of each class in the VHR image;

(2) Elimination of mixed pixels in latent training samples through binary edge and NDVI thresholds;

(3) Calculation of the parameters of training samples extracted from the previous step.

In step 1, the location of correctly classified pixels is obtained through a comparison between the attributes of the MDM and the classification result of the Landsat image. Then, latent training samples of each class in the VHR image are extracted by using the derivative location. However, they still include not only the feature of the desired class but also different features due to the difference of spatial resolution between the Landsat image and VHR images as illustrated in Fig. 3 (Section 3.3). Removal of other classes in the specific training sample is required to obtain pure pixels in the automated sampling procedure.

In step 2, the mixed pixels that occurred at step 1 can be removed by applying the binary edge and NDVI thresholds. The binary edge can extract the built-up feature well because built-up features are thin and small in the VHR image of non-accessible areas. Therefore, built-up features in this specific class can be effectively removed or included by choice of the binary edge threshold according to need. In the case of the NDVI, it is effective in identifying forest, water, and built-up features as described in Section 3.5. In particular, the FT is necessary to separate the forest feature from grass and crop features. The threshold options for each feature are shown in table 3. A filtering procedure for mixed pixels is conducted based on

these options, and training samples of each class are finally extracted. Through these processes, the proposed method is able to increase the purity of the training samples of each class.

In step 3, parameters, such as covariance and mean values, of training samples extracted from the previous step are calculated before MLC of the VHR image. Then, the MLC of the VHR image is started using the training parameters extracted.

Table 3. Threshold of binary edge and NDVI

Class	Built-up	Water	Crop	Grass	Forest
Edge Threshold	= 255	≠ 255	≠ 255	≠ 255	≠ 255
NDVI Threshold	< 0	< 0	< FT	< FT	≥ FT

4. Results and discussion

Two different scenes from two different sensors were used to validate the proposed method. Statistics of the training samples extracted through the automated sampling method were measured. Then, the classification results were validated through a visual interpretation and quantitative assessment.

4.1 Statistics of extracted training data

The number of training pixels, mean values, and separability of each class were calculated for training samples extracted from site 1 and site 2. Table 4 shows the number of pixels in training sets obtained through the automated sampling method. In order to analyse the statistics, other training samples were extracted through the manual method, and mean values were calculated for site 1 and site 2 (tables 5 and 6). Although there was little difference between mean values of the two methods for site 1, a similar tendency of mean values was confirmed. On the other hand, both mean values extracted from site 2 were very similar for all classes.

Table 4. Number of pixels in the training set of each class

Class	Site 1	Site 2
Built-up	10433	29794
Water	24657	5191
Crop	395012	1246158
Grass	930943	-
Forest	867686	197402

Table 5. Mean values of site 1

Class	Automatic				Manual			
	Band 1	Band 2	Band 3	Band 4	Band 1	Band 2	Band 3	Band 4
Built-up	1619	1567	1346	586	1865	1853	1818	592
Water	649	588	483	245	782	422	267	233
Crop	532	701	358	824	414	625	243	937
Grass	458	650	321	801	450	670	279	875
Forest	77	109	34	599	80	111	49	603

Table 6. Mean values of site 2

Class	Automatic				Manual			
	Band 1	Band 2	Band 3	Band 4	Band 1	Band 2	Band 3	Band 4
Built-up	119	116	76	90	124	118	72	87
Water	79	59	28	37	81	61	20	23
Crop	112	122	79	105	110	121	76	113
Forest	80	63	97	74	80	63	100	76

Additionally, we measured the separability between classes using the Jeffries-Matusita (JM) distance. The JM distance estimates the separability of a pair of probability distributions. A JM distance of 2.0 between spectral classes would imply classification of pixel data into those classes, assuming they were the only two, with 100% accuracy (Kailath 1967). The values of JM distance of the training sets are in tables 7 and 8. For site 1, separability between most classes was high except between crop features and grass features that have similar spectral characteristics in the image because the acquisition time of the QuickBird image was in summer. Therefore, they showed a low value of JM distance. For site 2, we confirmed that all classes had high values of JM distance. This means that the training samples extracted through the automated sampling method are appropriate to classify the experimental data.

Table 7. JM distance of site 1

Class	Built-up	Water	Crop	Grass	Forest
Built-up	0	1.6557	1.6022	1.8173	1.9910
Water	1.6557	0	1.9089	1.9859	1.9998
Crop	1.6022	1.9089	0	0.2919	1.9420
Grass	1.8173	1.9859	0.2919	0	1.8802
Forest	1.9910	1.9998	1.9420	1.8802	0

Table 8. JM distance of site 2

Class	Built-up	Water	Crop	Forest
Built-up	0	1.899	1.261	1.971
Water	1.899	0	1.904	1.991
Crop	1.261	1.904	0	1.991
Forest	1.971	1.991	1.991	0

4.2 Visual interpretation

VHR images were classified by using the training samples extracted in the previous step. Fig. 7(a) is the result applied to the QuickBird image of site 1, and Fig. 7(b) is the result applied to the SPOT-5 image of site 2. In site 1, built-up, water, grass, and forest features were well classified. According to the characteristics of VHR images, the result provided more detailed and accurate information than the MDM. However, the crop feature was misclassified into the grass class because they have similar spectral characteristics during summer. In site 2, the proposed method showed good performance for all features except the forest feature. The forest feature in shadow was classified to the water class because they have spectral characteristics similar to the water feature.

Fig. 8 shows magnified areas of the original images, MDM, and results of the proposed method for comparison. In Fig. 8(a) and 8(b), we can confirm that the proposed method pro-

vides more detail and accurate information than the MDM in situations such as the boundary between land and water and the density of forest, which are necessary for military operations. In addition, new attributes were assigned for areas that do not have attributes in the MDM (Fig. 8(c)).
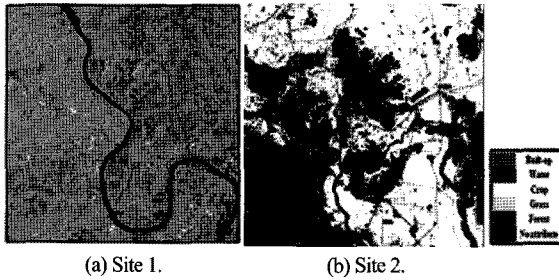

(a) Site 1.   (b) Site 2.

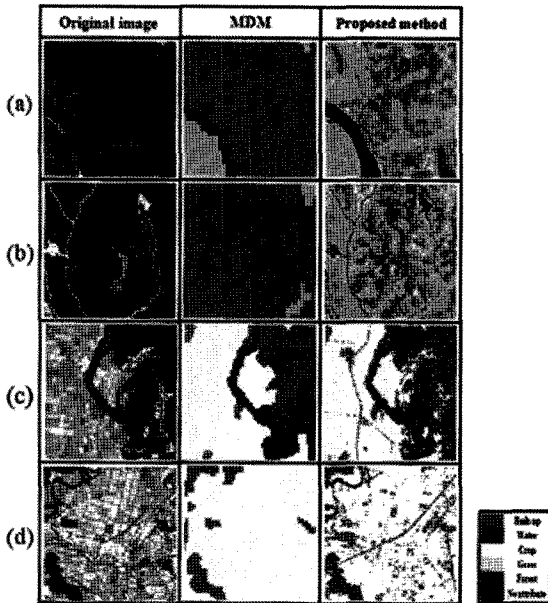**Fig. 7. Result of the proposed method.**

Fig. 8. Four magnified sections of the original images, MDM, and results of the proposed method.

4.3 Quantitative assessment

It is necessary to compare the remote sensing-derived classification map with what is called reference test information for classification accuracy assessment (Jensen 1996). To conduct our quantitative assessment, we chose a photo-interpretation approach rather than a field survey method to verify the proposed method because of the access constraints; 3340 reference points in the QuickBird image of site 1 and 2087

points in the SPOT-5 image of site 2 were extracted. Then, we compared our method with the manual method that is usually used in the supervised classification. The classification accuracies are listed in tables 9-12, which compare the results from the proposed and manual methods.

In terms of the accuracy assessments, the overall accuracy and Kappa coefficient of the manual method for site 1 were respectively 84.66% and 0.81 (table 9). The overall accuracy and Kappa coefficient of the proposed method were respectively 83.47% and 0.79 (table 10). The proposed method showed similar accuracy to the manual method. In the cases of built-up, water, and forest classes, high accuracies were seen, while crop and grass classes had relatively low accuracies including commission and omission errors due to their spectral characteristics. Crop and grass features have similar spectral characteristics during the summer season and this led to a low separability between crops and grass. This situation was also evident in the results of the manual method. In the case of site 2, the overall accuracy and Kappa coefficient of the manual method were respectively 94.15% and 0.91 (table 11). The overall accuracy and Kappa coefficient of the proposed method were respectively 88.98% and 0.85 (table 12). The two methods appeared to provide high overall accuracy. The principal reason is that the SPOT-5 image was taken during autumn and homogeneity was increased due to the lower spatial resolution of the SPOT-5 image. In addition, separability among all classes was better at site 2 than at site 1 because there were four classes but no grass class in the MDM. Therefore, the proposed method showed good performance for site 2.

5. Conclusion

We have suggested a new classification method based on automatic extraction of training samples for the land cover classification of VHR imagery. The proposed method could be effective, saving time and generating objective results through the exclusion of an intervening operator. In addition, the use of commercially available VHR images, QuickBird, and SPOT-5 could provide more detailed and accurate information for military operations in non-accessible areas.

In order to automate the training procedure, we determined

Table 9. Confusion matrix of manual method for site 1

	Built-up	Water	Crop	Grass	Forest	User's Accuracy (%)
Built-up	773	2	0	10	0	98.47
Water	0	418	18	0	0	95.87
Crop	2	0	225	388	0	36.59
Grass	0	0	68	541	17	86.42
Forest	0	0	1	9	886	98.88
Producer's Accuracy (%)	99.74	99.52	72.12	57.07	98.12	84.66(Overall)

Table 10. Confusion matrix of proposed method for site 1

	Built-up	Water	Crop	Grass	Forest	User's Accuracy (%)
Built-up	732	0	0	11	0	98.52
Water	39	418	15	0	0	88.56
Crop	3	2	129	176	2	41.35
Grass	1	0	168	758	135	71.37
Forest	0	0	0	3	766	99.61
Producer's Accuracy (%)	94.45	99.52	41.35	79.96	84.83	83.47(Overall)

Table 11. Confusion matrix of manual method for site 2

	Built-up	Water	Crop	Forest	User's Accuracy(%)
Built-up	483	40	22	32	83.71
Water	0	249	0	1	99.60
Crop	20	0	462	2	95.45
Forest	2	3	0	771	99.36
User's Accuracy (%)	95.64	85.27	95.45	95.66	94.15(Overall)

Table 12. Confusion matrix of proposed method for site 2

	Built-up	Water	Crop	Forest	User's Accuracy(%)
Built-up	464	2	7	50	88.72
Water	38	289	4	106	72.25
Crop	2	1	473	19	89.08
Forest	1	0	0	631	99.68
Producer's Accuracy (%)	91.88	98.97	97.73	78.29	88.98(Overall)

the threshold of the NDVI and binary edge appropriate to obtain the pure samples of each class. Then, visual interpretation and quantitative assessment of the results were conducted to validate the proposed method against a manual method. The overall accuracies of the two experimental sites were 83.47% and 88.98% and the Kappa coefficients were 0.79 and 0.85 for site 1 and site 2. This accuracy indicates that the proposed method could be used to provide detailed information for military operations. In addition, the proposed method showed good performance in terms of updating areas that do not have attributes in the MDM. Therefore, we expect that the proposed method can be used effectively to automatically

construct thematic maps for non-accessible areas.

Through the experiments with various satellite images, it was concluded that this method can be applied without exception when using a variety of VHR satellite sensors. However, this method tended to demonstrate low accuracy in terms of classification between crops and grass classes during the summer season because of their similar spectral characteristics. Therefore, in order to solve this problem, future work will focus on raising the separability between these two classes by integrating other methods, such as object-oriented and texture-based approaches.

Acknowledgement

References

Barnsley, M.J. and Barr S.L., (1996), Inferring urban land use from satellite sensor images using kernel-based spatial reclassification, *Photogrammetric Engineering and Remote Sensing*, 62, pp. 949-958.

Chen, D.M. and Stow, D., (2003), Strategies for integrating Information from multiple spatial resolutions into land-use/land-cover classification routines, *Photogrammetry Engineering and Remote Sensing*, 69, pp. 1279-1287.

Davis, C.H. and Wang, X., (2002), Urban land cover classification from high resolution multi-spectral IKONOS imagery, In *IGARSS Toronto, ON, Canada*, June 24-28, 2, pp. 1204-1206.

Di, K., Li, D. and Li, D., (2000), Land use classification of remote sensing image with GIS databased on spatial data mining techniques, *International Archives of Photogrammetry Remote Sensing*, 33, pp. 238-245.

Eo, Y.D., (1999), Development of the training normalization algorithm and the class separability measurement for satellite image classification. PhD thesis, Seoul National University, South Korea.

Eo, Y.D., Lee, G.W., Park, D.Y., Park, W.Y. and Lee, C.N., (2008), Supervised Classification Using Training

Parameters and Prior Probability Generated from VITD - The Case of QuickBird Multispectral Imagery, Korean Journal of Remote Sensing, 24, pp. 517-524.

Haiping, S., Duarne K., Eric, F., Michael, F., Rose, D., Jeffrey, S.M., Bruce, C., Lawrence, R.H. and Thomas, M., (2006), Evaluation of eelgrass beds mapping using a high-resolution airborne multispectral scanner, *Photogrammetry Engineering and Remote Sensing*, 72, pp. 789-797.

Han, D.I. and Lee, B.M., (2006), Development of Early Tunnel Fire Detection Algorithm Using the Image Processing, *In International Symposium on Visual Computing*, LNCS4292, pp. 39-48.

Huang, X., Zhang, L. and Li, P., (2007), Classification and extraction of spatial features in urban areas using high-resolution multispectral imagery, *IEEE Geoscience Remote Sensing Letter*, 4, pp. 260-264.

Jensen, J., 1996, Intoroductory Digital Image Processing : A remote Sensing Perspective, Second Edition, p. 305.

Kailath, T., (1967), The divergence and Bhattacharyya distance measures in single selection, *IEEE Transaction Communication Theory*, 15, pp. 52-60.

Kim, W.S., Yun, K.H., Heo, J. and Jayakumar, S., (2008), The Expectation of the Land Use and Land Cover Using CLUE-S Model and Landsat Images, *The Korean Society for Geo-Spatial Information System*, 16, pp. 33-41.

Kim, Y.M., Kim, Y.I., Eo, Y.D. and Park, W.Y., (2009a), Automatic classification of high resolution multispectral images for GIS data revision of non-accessible areas, In International Symposium on Remote Sensing, 28-30 October 2009, Pusan, South Korea, pp. 19-22.

Kim, Y.M., Byun, Y.G., Kim, Y.I. and Eo, Y.D., (2009b), Detection of Cochlodinium polykrikoides red tide based on two-stage filtering using MODIS data, *Desalination*, 249, pp. 1171-1179.

Martinuzzi, S., Gould, W.A., Ramos Gonzalez, O.M., Robels, A.M., Maldonado, P.C., Perez-buitrrago, N. and Fimero caban, J.J., (2008), Mapping tropical dry forest habitats integrating Landsat NDVI, Ikonos imagery, and topographic information in the Caribbean Island of Mona, *Revista de Biologia Tropical*, 56, pp. 625-639.

Maselli, F., Conese, C., Petkov, L. and Resti, R., (1992), Inclusion of prior probabilities derived from a nonparamet-

ric process into the maximum likelihood classifier, *Photogrammetry Engineering and Remote Sensing*, 58, pp. 201-207.

Maselli, F., Gardin, L. and Bottai, L., (2008), Automatic mapping of soil texture through the integration of ground, satellite and GIS data, *International Journal of Remote Sensing*, 29, pp. 5555-5569.

Park, W.Y, Song, H.S., Heo, J., Eo, Y.D., Kim, Y.M. and Jang, A.J., (2009), The Comparative study between MODIS satellite image product and military tree canopy cover property, *In symposium of The Korea Institute of Military Science and Technology*, Jeju, South Korea, No. 202.

Peters, A.J. and Eve, M.D., (1995). Satellite monitoring of desert plant community response to moisture availability, *Environmental Monitoring and Assessment*, 37, pp. 273-287.

Ricchetti, E., (2000), Multispectral satellite image and GIS data integration for geological classification, *Photogrammetry Engineering and Remote Sensing*, 66, pp. 429-435.

Rouse, J.W., Haas Jr., R.H., Schell, J.A. and Deering, D.W., (1974), Monitoring vegetation systems in the great plains with ERTS, In: NASA SP-351, 3rd ERTS-1 Symposium, Washington, DC, pp. 309-317.

Tarantino, C., Daddabbo, A., Astellana, L., Pasquariello, G. , Blonga, P. and Satalino, G., (2003), Extraction of urban settlements by an automatic approach on high resolution remote sensed data, *In IEEE International Conference Geoscience Remote Sensing*, 3, pp. 1975-1977.

Walter, V., (1998), Automatic classification of remote sensing data for GIS database revision, *International Archives of Photogrammetry Remote Sensing*, 32, pp. 641-648.

Wang, Q. and Tenhunen, J.D., (2004), Vegetation mapping with multitemporal NDVI in North Eastern China Transect (NECT), International Journal of Applied Earth Observation and Geoinformation, 6, pp. 17-31.

Yang, X., (2007), Integrated use of remote sensing and geographic information systems in riparian vegetation delineation and mapping, *International Journal of Remote Sensing*, 28, pp. 353-370.

Zhu, C., Shi, W., Pesaresi, M., Liu., I., Chen, X. and King., B., (2005), The recognition of road network from high-resolution satellite remotely sensed data using image morphological characteristics, *International Journal of Remote Sensing*, 26, pp. 5493-5508.

Zijdenbos, A., Forghani, R. and Evans, A.C., (1998), Automatic quantification of MS lesions in 3D MRI brain data sets: Validation of INSECT. In: Wells, W.M., Colchester, A.C.F., Delp, S. (Eds.), MICCAI'98., 1496 of LNCS. Springer, Berlin, pp. 439-448.

Zijdenbos, A.P., Forghani, R. and Evans A.C., (2002), Automatic 'pipeline' analysis of 3D MRI data for clinical trials: application to multiple sclerosis, *IEEE Transaction Medical Imaging*, 21, pp. 1280-1291.